Edinburgh Research Explorer

Propagation of optical spatial solitary waves in bias-free nematic-liquid-crystal cells

OPEN ACCESS

Propagation of optical spatial solitary waves in bias-free nematic-liquid-crystal cells

Antonmaria A. Minzoni,[1] Luke W. Sciberras,[2] Noel F. Smyth,[3] and Annette L. Worthy[2]

[1]*Fenomenos Nonlineales y Mecánica (FENOMEC), Department of Mathematics and Mechanics, Instituto de Investigación en Matemáticas Aplicádas y Sistemas, Universidad Nacional Autónoma de México, 01000 México D.F., México*

[2]*School of Mathematics and Applied Statistics, University of Wollongong, Northfields Avenue, Wollongong, New South Wales 2522, Australia*

[3]*School of Mathematics and Maxwell Institute for Mathematical Sciences, University of Edinburgh, Edinburgh EH9 3JZ, Scotland, U.K.*

The propagation of a bulk optical solitary wave in a rectangular cell filled with a nematic liquid crystal—a nematicon—is mathematically modelled. In order to overcome the Freédricksz threshold the cell walls are rubbed to pretilt the nematic. A modulation theory, based on a Lagrangian formulation, is developed for the $(2 + 1)$-dimensional propagation of the solitary wave beam down the cell. This modulation theory is based on two different formulations of the director distribution. The relative advantages and disadvantages of these two methods are discussed. A previously unexplored method based on images is found to possess significant advantages. Excellent agreement with full numerical solutions of the nematicon equations is found for both methods. Finally, the implications of the results obtained for some widely used approximations to the nematicon equations are discussed, particularly their use in comparisons with experimental results.

I. INTRODUCTION

A nematic liquid crystal is an ideal medium in which to study the propagation of nonlinear beams. It possesses a "huge" nonlinearity, so that nonlinear effects can be observed over millimeter distances. Furthermore, the response of a liquid crystal is termed nonlocal as the response of the nematic medium to a coherent beam of light extends far beyond the beam's waist. It is this nonlocal response that stops the usual catastrophic collapse of two-dimensional bulk solitary waves [1–3]. Since the first experimental observation of a bulk solitary wave in a nematic liquid crystal [4], termed a nematicon, there has been much subsequent experimental [2,5–7] and theoretical [1,8–10] research on nematicons and other bulk solitary waves in nonlinear, nonlocal media [11–18]. In these media the intensity-dependent enhancement of the refractive index, resulting in self-focusing, can balance diffraction, so that a self-sustaining solitary wave can form. In nematic liquid crystals the change in refractive index is due to the rotation of the nematic molecules, the refractive index being different parallel and perpendicular to the nematic axis, the director. Interest in nonlinear beams in nematic liquid crystals has centered on their potential as the basis for all-optical devices [2,7,13]; for example, reconfigurable waveguides. In nematic liquid crystals there exists a phenomenon termed the Freédricksz threshold, whereby there exists a power threshold to overcome the elastic inertia forces and cause the nematic molecules to rotate [19]. To enable nematicons to form from milliwatt beams this threshold is overcome in two ways. The first is that an external static electric field is applied to pretilt the molecules [1,2]. The second is that the walls of the nematic cell are "rubbed" so that the nematic molecules are pretilted at an angle at the walls. Elastic forces then propagate this pretilt throughout the bulk medium. It is the second pretilting mechanism of rubbing that will be the basis of the present work.

The major physical difference between the two pretilting mechanisms is that, when an external static electric field is applied, the director re-orientation decays exponentially away from the beam [20]. Because a typical ratio of the cell to beam width is $O(20)$, the effect of the cell walls on the nematicon can usually be neglected if the nematicon is launched near the center of the cell. However, in the case of pretilting by rubbing, the re-orientation behaves logarithmically so that the effect of the cell walls cannot be neglected [20,21]. The effect of the cell walls on nematicon motion was considered experimentally by Alberucci *et al.*, [22] and theoretically by Alberucci *et al.*, [21]. The major effect of the cell walls is that they are repulsive, so that a nematicon "bounces" around the cell as it propagates down it. The theoretical work considered the cell to be infinite in the direction transverse to the direction down the cell and the polarization direction of the beam. It used a Fourier series approach to obtain approximate equations for the nematicon trajectory. A modulation-theory approach, based on averaged Lagrangians, was used to theoretically model the propagation of a one-dimensional nematicon down a finite cell [20]. This approach differed from that of Alberucci *et al.* [21] in that the coupling between the nematicon trajectory and its amplitude and width evolution was included. It also used an exact solution for the director distribution based on a trial function for the beam profile. A similar, theoretical modulation-theory approach will be used in the present work to study the propagation of a nematicon in a full two-transverse-dimensional cell. The present work differs from that of Alberucci *et al.*, [21] in that the cell will be taken to be finite in both directions orthogonal to the direction down the cell and the coupling between the amplitude and width evolution of the nematicon and its trajectory will be included. Lastly, and importantly, the effect of the diffractive radiation shed by the nematicon as it evolves will be incorporated.

The present work considers the effect of cell boundaries on the propagation of a single nematicon, which is the lowest-order ground-state solitary wave. If higher-order excited-state solitary waves or vortices are considered, the interaction between the beam and the boundaries becomes more involved as it can transform between different states with different

geometries [23]. As well as the walls encasing the liquid crystal, internal boundaries can be introduced into the cell [24]. These act to locally change the refractive index of the liquid crystal and refract the beam, which is a different effect from the repulsion of the cell boundaries. The interaction of multiple nematicons, both co- and counterpropagating, in a finite liquid-crystal cell introduces further complications because the propagation of the beams now depends on both the repelling effect of the boundaries and the interbeam interaction, which is mediated via the nonlocal response of the nematic [25,26].

Recently, good agreement between experimental and numerical results has been found if the Fourier series solution for the director distribution is truncated at the fundamental mode [27,28]. This approximation has been found useful to study nonparaxial contributions to a nematicon's evolution. The full Fourier series solution of the present work will be used to show why this approximation works well for the nematicon's trajectory, but not its profile evolution. Finally, an alternative method of images solution [29] for the director distribution will be used to study the evolution of a nematicon down a finite cell. The relative advantages of the Fourier series and method of images solutions will be discussed. A major result is that the method of images solution requires far fewer terms to give accurate results. In particular, including the inner-most 8 images gives good agreement with numerical solutions, demonstrating the local effect of the cell boundary on the bouncing of the nematicon. This indicates that the method of images can be a useful alternative to the usual Fourier series methods [21,22].

II. GOVERNING EQUATIONS

Let us consider the propagation of a coherent, linearly polarized light beam input into a planar liquid-crystal cell. Let us define a coordinate system with the x direction in the polarization direction, the z direction down the cell, and the y direction orthogonal to these two directions. To enable optical solitary waves, so-called nematicons [2], to form from milliwatt input beams, the nematic molecules need to be pretilted to overcome the Freédricksz threshold [1,19], otherwise the beam will diffract and not form a nematicon. This pretilt can be achieved using two main mechanisms. The first of these is that an external static electric field is applied to rotate the molecules to a pretilt angle θ_0 [1]. Usually $\theta_0 \sim \pi/4$ as the Freédricksz threshold is zero for $\theta_0 = \pi/4$ [1]. The other method is to "rub" the nematic cell so that the nematic molecules are at an angle θ_0 to the cell walls. The elastic response of the nematic results in this angle being transmitted to the bulk of the nematic. Both of these pretilt mechanisms result in the bulk nematic being pretilted at an angle θ_0 to the z direction. The electric field of the light beam then results in an additional rotation θ of the nematic director. For the milliwatt power levels of these beams, $|\theta| \ll |\theta_0|$. In this small-deviation limit the nondimensional equations governing the propagation of the beam through the liquid-crystal cell are [20–22]

$$i\frac{\partial E}{\partial z} + \frac{1}{2}\nabla^2 E + 2E\theta = 0, \tag{1}$$

$$\nu\nabla^2\theta = -2|E|^2. \tag{2}$$

The Laplacian ∇^2 is in the (x,y) plane in the paraxial approximation [1,2,30]. The variable E is the complex-valued slowly varying envelope of the optical field. The parameter ν measures the strength of the elastic response of the nematic, with a large value of ν corresponding to a nonlocal response [1]. Typically ν is $O(100)$ in experiments [31]. It should be noted that the Poynting vector walk off has been taken out of the nonlinear Schrödinger (NLS) equation (1) by the use of a phase factor [32,33], which is valid as the nematic has constant properties and so the walk off is constant [33]. In the NLS-type equation (1) the z coordinate is a time-like coordinate. As the usual cell geometry is rectangular, let us take the cell to lie in $0 \leqslant x \leqslant L_x$ and $0 \leqslant y \leqslant L_y$. In experimental studies of the effect of cell boundaries on nematicon propagation, a typical cell thickness was 75 μm with a typical beam waist of 3 μm for a 1.064 μm beam [32]. A typical nondimensional cell dimension is then 25. A typical beam power was 3 mW [32]. Since the nematic molecules are fixed at the angle θ_0 at the cell walls, the appropriate boundary conditions for the perturbation angle θ are $\theta = 0$ on the four walls $x = 0, L_x$, and $y = 0, L_y$. Equations (1) and (2) are generic and also arise in nonlinear beam propagation in thermal media [14–16] and certain photorefractive crystals [17,18].

The nematicon equations (1) and (2) have the Lagrangian

$$L = i(E^*E_z - EE_z^*) - |\nabla E|^2 + 4\theta|E|^2 - \nu|\nabla\theta|^2. \tag{3}$$

Here, the superscript * denotes the complex conjugate. Alternatively, the director equation (2) can be solved in terms of a Green's function $G(x,y,x',y')$

$$\theta = -\frac{2}{\nu}\int_0^{L_y}\int_0^{L_x}|E(x',y')|^2 G(x,y,x',y')dx'dy' \tag{4}$$

and the result substituted into the electric field equation (1) to yield a single equation governing the nematicon. The Lagrangian for the electric field equation (1) in this case is then

$$L = i(E^*E_z - EE_z^*) - |\nabla E|^2$$
$$- \frac{4}{\nu}|E|^2\int_0^{L_y}\int_0^{L_x}|E(x',y')|^2 G(x,y,x',y')dx'dy'. \tag{5}$$

The Lagrangian (3) will be used to develop the modulation equations when the director equation (2) is solved using Fourier series, while the Lagrangian (5) will be used for the modulation equations based on using an images solution for the Green's function G.

III. EVOLUTION EQUATIONS

The nematicon equations (1) and (2) have no known exact solitary wave, or nematicon, solution for general values of the nonlocality ν. In this case, approximate techniques, many based on averaged Lagrangian methods [34], have proved successful in obtaining solutions in excellent agreement with numerical and experimental results and, furthermore, have offered insights into mechanisms and the underlying physics not available from numerical solutions alone [30,31,33,35–40]. A hybrid of exact solutions and averaged Lagrangian techniques will be used in this work, as in [20].

As there is no known exact nematicon solution, the modulation theory will be based on a suitable trial function for this unknown profile [30]. Indeed, in many applications the features of the nematicon evolution, such as its trajectory, have been found to be independent of the choice of trial function for its profile [38,39]. The two main choices for this trial function are sech and Gaussian profiles, with sech being the exact soliton solution for the one-dimensional NLS equation and a Gaussian being the limiting profile of a nematicon in the limit of infinite nonlocality ν [41]. It has been shown that, around its peak, a nematicon has a Gaussian profile, while in its tails it has the exponential decay of the modified Bessel function K_0, which is more similar to the decay of sech [1]. In the present work the Gaussian trial function

$$E = \left(a e^{-\frac{r^2}{w^2}} + i g\right) e^{i\psi} \tag{6}$$

will be used, where

$$r^2 = (x - \xi)^2 + (y - \eta)^2, \tag{7}$$

$$\psi = \sigma + V_x(x - \xi) + V_y(y - \eta). \tag{8}$$

It should be noted that this trial function is radially symmetric. Experimental results show that a nematicon has a slight elliptic cross section [7], which is neglected in order to keep the modulation theory and the resulting modulation equations as simple as possible. The amplitude a, width w, position (ξ, η), propagation constant (V_x, V_y), phase σ, and g are functions of z. The first term in Eq. (6) represents a varying nematicon-like beam. The second term represents the shelf of low-wave-number diffractive radiation which accumulates under the evolving nematicon [30,42]. In the case of the $(1 + 1)$-dimensional $[(1 + 1)D]$ NLS equation the existence of this shelf of radiation has been shown from perturbed inverse scattering theory [42], while for a coupled system of NLS equations and for the defocusing NLS equation it has been shown using perturbation theory [43–45]. However, the reason for this shelf of radiation is most easily seen from the following physical argument: The dispersion relation for the linearized electric field equation (1) is $\omega = |\mathbf{k}|^2/2$, so that the group velocity is $\mathbf{c}_g = \mathbf{k}$. Low-wave-number (long-wavelength) waves then have low group velocity and so accumulate under the evolving nematicon. The shelf is $\pi/2$ out of phase with the nematicon as the in-phase perturbations serve to change the amplitude and width of the nematicon [42]. The variable g is the height of this radiation shelf. Optical power cycles into and out of the shelf, resulting in the nematicon's amplitude and width oscillating as it evolves. This shelf of radiation cannot remain flat indefinitely, so it is assumed that g is nonzero in the disk $(x - \xi)^2 + (y - \eta)^2 \leqslant \ell^2$.

In previous work the director response was approximated by a trial function with a sech^2 profile [30]. This was a good approximation as the director was pretilted by an external static electric field, which caused the director response due to the beam to decay exponentially away from it. However, when there is no pretilting field the director response behaves logarithmically away from the beam, as may be found from the director equation (2) on setting $E = 0$. This different decay of the beam and the director response can be seen in Fig. 1. In this case it is better to solve the director equation (2) exactly, as found in previous work for a one-dimensional
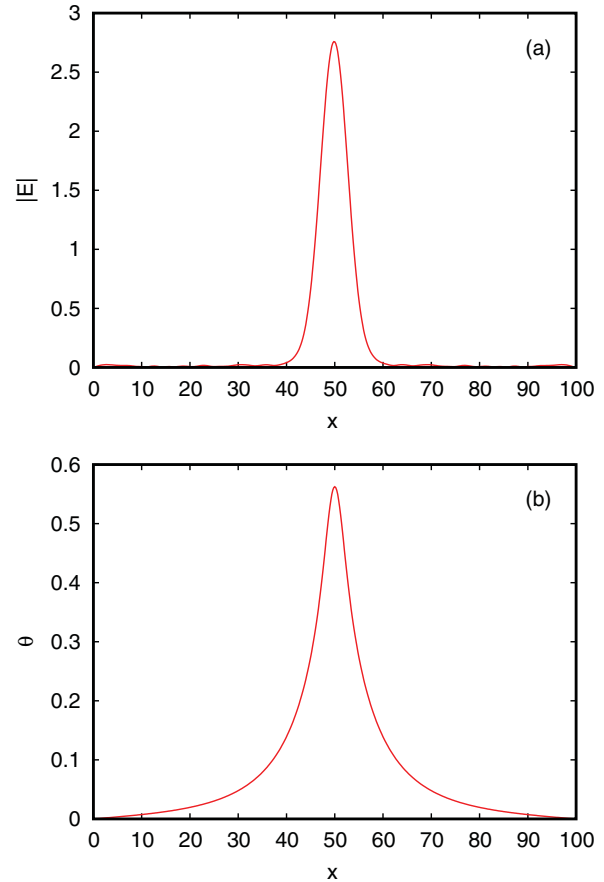

FIG. 1. (Color online) Electric field intensity versus x. Shown are the numerical solutions for (a) $|E|$ and (b) θ for $y = 0$ at $z = 500$. The initial values are $a = 2.5$, $w = 4$, $\xi = 50$, and $\eta = 5$ with $\nu = 200$, $L_x = 100$, and $L_y = 50$.

nematicon [20]. In the present work the director equation will now be solved using two methods: a Fourier series solution and a solution based on using the method of images to find the Green's function for the Laplacian, which occurs in the Lagrangian (5).

A. Fourier series expansion

The director equation (2) has an exact solution using an eigenfunction expansion, a Fourier series, on substituting the trial function (6) for E. After neglecting the $O(g^2)$ contribution, this solution is

$$\theta = -\sum_{n=1}^{\infty} \sum_{m=1}^{\infty} \frac{C_{nm}}{\pi^2 Q_1} \sin \frac{n\pi x}{L_x} \sin \frac{m\pi y}{L_y}, \tag{9}$$

where the Fourier coefficients are

$$C_{nm} = -\frac{4\pi a^2 w^2}{\nu L_x L_y} e^{-\gamma_1} \sin \frac{n\pi \xi}{L_x} \sin \frac{m\pi \eta}{L_y}, \tag{10}$$

$$Q_1 = \frac{n^2}{L_x^2} + \frac{m^2}{L_y^2}, \quad \gamma_1 = \frac{\pi^2 Q_1 w^2}{8}. \tag{11}$$

The trial function (6) and the solution (9) for the director θ are now substituted into the Lagrangian (3), which is then

averaged by integrating in x and y over the cell [34] to yield the averaged Lagrangian

$$\mathcal{L} = -2\left(\frac{1}{4}a^2w^2 + \Lambda g^2\right)\left(\sigma' - V_x\xi' - V_y\eta'\right)$$
$$+ \frac{1}{2}V_x^2 + \frac{1}{2}V_y^2\right) - aw^2g' + gw^2a' + 2agww'$$
$$- \frac{1}{2}a^2 + \frac{2a^4w^4}{\pi\nu L_xL_y}\sum_{n=1}^{\infty}\sum_{m=1}^{\infty}\frac{e^{-2\gamma_1}}{Q_1}\sin^2\frac{n\pi\xi}{L_x}\sin^2\frac{m\pi\eta}{L_y}.$$
(12)

Here $\Lambda = \ell^2/2$, which is the area under the shelf, modulo 2π. Taking the variations of this averaged Lagrangian with respect to the nematicon parameters gives the modulation equations for the nematicon evolution. These modulation equations are given in Appendix A.

The equation for total energy conservation can be found from Nöther's theorem based on invariances of the Lagrangian (3) with respect to shifts in z. Averaging this energy conservation equation by integrating over the cell in x and y gives the averaged energy conservation equation

$$\frac{dH}{dz} = \frac{d}{dz}\int_0^{L_y}\int_0^{L_x}[|\nabla E|^2 - 4\theta|E|^2 + \nu|\nabla\theta|^2]dxdy$$
$$= \frac{d}{dz}\left[\frac{a^2}{2} - \frac{2a^4w^4}{\pi\nu L_xL_y}\sum_{n=1}^{\infty}\sum_{m=1}^{\infty}\frac{e^{-2\gamma_1}}{Q_1}\right.$$
$$\left. \times \sin^2\frac{n\pi\xi}{L_x}\sin^2\frac{m\pi\eta}{L_y}\right] = 0.$$
(13)

This energy conservation equation can be used to determine the final steady nematicon for a given input beam. Due to the repulsion effect of the cell walls [21,22] the equilibrium position of the nematicon is at the center of the cell. If we denote steady state values by a caret, we then have $\hat{V}_x = \hat{V}_y = 0$, $\hat{\xi} = L_x/2$, and $\hat{\eta} = L_y/2$. The modulation equation (A9) for g gives the relation

$$\hat{a}^2 = \frac{\nu L_xL_y}{\pi\hat{w}^6}\left[\sum_{n=1}^{\infty}\sum_{m=1}^{\infty}e^{-2\hat{\gamma}_1}\right]^{-1}$$
(14)

between the amplitude and width of the nematicon at the steady state. The energy equation (13) can then be used in conjunction with this relation to determine the steady amplitude and width for a given input beam.

B. Method of images

The Green's function G in the Green's function solution (4) for the director distribution θ can be determined using the method of images [29]. This involves using the point source solution for the Laplacian on the infinite plane (x, y), with the source sited at the point (x', y') in the cell, and then using appropriately signed images of this point source solution in the boundaries of the cell so that the sum of all the sources satisfies the zero boundary condition on the cell walls. The Green's function is then given by [29]

$$G = -\frac{1}{2\pi}\text{Re}\left\{\ln\frac{\sigma(h-\mu,x,y)\sigma(h+\mu,x,y)}{\sigma(h-\mu^*,x,y)\sigma(h+\mu^*,x,y)}\right\},$$
(15)

where

$$h = x + iy, \quad \mu = x' + iy',$$
$$\sigma(u,x,y) = u\prod_{\omega\neq 0}\left[\left(1-\frac{u}{2\omega}\right)e^{u/(2\omega)+u^2/(8\omega^2)}\right].$$
(16)

Then u is a complex valued function and

$$\omega = nL_x + imL_y, \quad n = 0, \pm1, \ldots, \quad m = 0, \pm1, \ldots.$$
(17)

This Green's function is the half plane Green's function mapped conformally onto a rectangle via the elliptic function σ [29]. The Green's function (15) is now substituted into the solution (4) for θ and (5) for the Lagrangian. However, the integral cannot be evaluated exactly. As in the nonlocal limit with ν large, the director response is much wider than the beam, the standard approximation can be made that the Green's function does not show significant variation over the beam [40,46]. In this case the solution (4) for the director perturbation θ can be approximated by

$$\theta = \frac{a^2w^2}{4\nu}\text{Re}\left\{\ln\frac{\sigma(h-\mu,x,y)\sigma(h+\mu,x,y)}{\sigma(h-\mu^*,x,y)\sigma(h+\mu^*,x,y)}\right\}.$$
(18)

The Green's function (15) is now substituted into the Lagrangian (5), which is averaged over the cell to give the averaged Lagrangian

$$\mathcal{L} = -2\left(\frac{1}{4}a^2w^2 + \Lambda g^2\right)\left(\sigma' - V_x\xi' - V_y\eta' + \frac{1}{2}V_x^2 + \frac{1}{2}V_y^2\right) - aw^2g' + gw^2a' + 2agww'$$
$$- \frac{a^2}{2} + \frac{a^4w^4}{4\nu}[-\Delta_1 - \Delta_2 + \Delta_3 + \Delta_4].$$
(19)

Here,

$$\Delta_1 = \ln\frac{w}{\sqrt{2}} - \frac{\gamma}{2} - \ln 2 + \ln\sqrt{\xi^2 + \eta^2} - \ln(\xi\eta),$$
(20)

$$\Delta_2 = \sum_{n,m=-\infty}^{\infty} \left[\frac{1}{2} \ln \frac{(nL_x - \xi)^2 + (mL_y - \eta)^2}{n^2 L_x^2 + m^2 L_y^2} + \frac{(\xi^2 - \eta^2)(n^2 L_x^2 - m^2 L_y^2) + 4nm\xi\eta L_x L_y}{2(n^2 L_x^2 + m^2 L_y^2)^2} \right], \tag{21}$$

$$\Delta_3 = \sum_{n,m=-\infty}^{\infty} \left[\frac{1}{2} \ln \frac{n^2 L_x^2 + (mL_y - \eta)^2}{n^2 L_x^2 + m^2 L_y^2} - \frac{\eta^2 (n^2 L_x^2 - m^2 L_y^2)}{2(n^2 L_x^2 + m^2 L_y^2)^2} \right], \tag{22}$$

$$\Delta_4 = \sum_{n,m=-\infty}^{\infty} \left[\frac{1}{2} \ln \frac{(nL_x - \xi)^2 + m^2 L_y^2}{n^2 L_x^2 + m^2 L_y^2} + \frac{\xi^2 (n^2 L_x^2 - m^2 L_y^2)}{2(n^2 L_x^2 + m^2 L_y^2)^2} \right], \tag{23}$$

where γ is Euler's constant, $\gamma = 0.577\,215\,665$. Taking variations of the averaged Lagrangian (19) with respect to the nematicon parameters gives the modulation equations for the evolution of the beam. These modulation equations are summarized in Appendix B.

The equation for total energy conservation can be derived using Nöther's theorem as for the Fourier series solution. With the director given by (18), the equation for energy conservation is

$$\frac{dH}{dz} = \frac{d}{dz} \int_0^{L_y} \int_0^{L_x} [|\nabla E|^2 - 2|E|^2 \theta] dx\, dy$$
$$= \frac{d}{dz} \left\{ \frac{1}{2} a^2 - \frac{a^4 w^4}{4\nu} [-\Delta_1 - \Delta_2 + \Delta_3 + \Delta_4] \right\} = 0. \tag{24}$$

The final steady state nematicon can again be determined from this energy conservation equation. The relationship between the steady state amplitude $\hat{a}$ and width $\hat{w}$ is given by the modulation equation (B6) for g as

$$\hat{a}^2 = \frac{4\nu}{\hat{w}^4}. \tag{25}$$

Thus for a given input beam, the energy conservation equation (24) then determines the equilibrium nematicon. Numerical computation gives excellent agreement for the equilibrium nematicon as given by the Fourier series method (13) and the images solution (24), as required.

The final parameter to be determined is the shelf radius ℓ. In previous studies the modulation equations were linearized about their fixed point, which resulted in a simple harmonic oscillator equation [35,42]. The frequencies this oscillator and the steady state nematicon were then matched to determine Λ [35,42]. However, this method does not work for the present finite cell modulation equations, as was found for a one-dimensional nematicon in a finite cell [20]. The reason is that the perturbation of the director angle θ does not form a localized distribution, as for an infinite cell with a pretilting external static electric field [20,30,35]; see Fig. 1. For the case of a one-dimensional nematicon this problem was overcome by matching the frequency of the nematicon's amplitude oscillation as given by the modulation equations and the full numerical solution for a particular input beam and then showing that this matched frequency was robust for different input beams [20]. The same method will be used here. We then take the shelf radius to be

$$\ell = \frac{3\beta\pi^2 \hat{w}}{8}, \tag{26}$$

where β is a constant to be determined. For $\beta = 1$ this expression is the shelf length for the NLS equation [42]. It was found that $\beta = 0.4$ gave a robust match for the period of the numerical solutions.

IV. RESULTS

In this section solutions of the modulation equations will be compared with full numerical solutions of the nematicon equations (1) and (2). The modulation equations were solved using the standard fourth-order Runge-Kutta method. The electric field equation (1) was solved using centered second-order differences for the Laplacian $\nabla^2 E$ and a second-order predictor-corrector method based on the second-order Runge-Kutta method to advance in z. The initial condition for the electric field was the trial function (6) with $g = 0$. The elliptic director equation (2) was solved using standard centered second order differences for the Laplacian $\nabla^2 \theta$ and then solving the resulting linear system using Jacobi iteration. The step sizes used were $\Delta x = \Delta y = 0.2$ and $\Delta z = 0.001$. Nondimensional cell dimensions of 50 and 100 were chosen, as these are of the order of typical experimental sizes, as discussed in Sec. II. A propagation distance of $z = 500$ was chosen as this is a typical nondimensional cell length [31].

Let us first consider the propagation of a nematicon in a square cell. While in experiments nematic cells have a rectangular profile, a square cell will be considered in order to examine the effect of the aspect ratio on the nematicon's evolution. Figure 2 shows a comparison between the full numerical solution and solutions of the modulation equations based on the Fourier series and method of images methods for such a square cell. It can be seen that there is an excellent comparison between the modulation solutions and the numerical solution for both the amplitude and position. There is a small period difference between the amplitude oscillations as given by the modulation and numerical solutions, with the Fourier series solution giving a period in better agreement
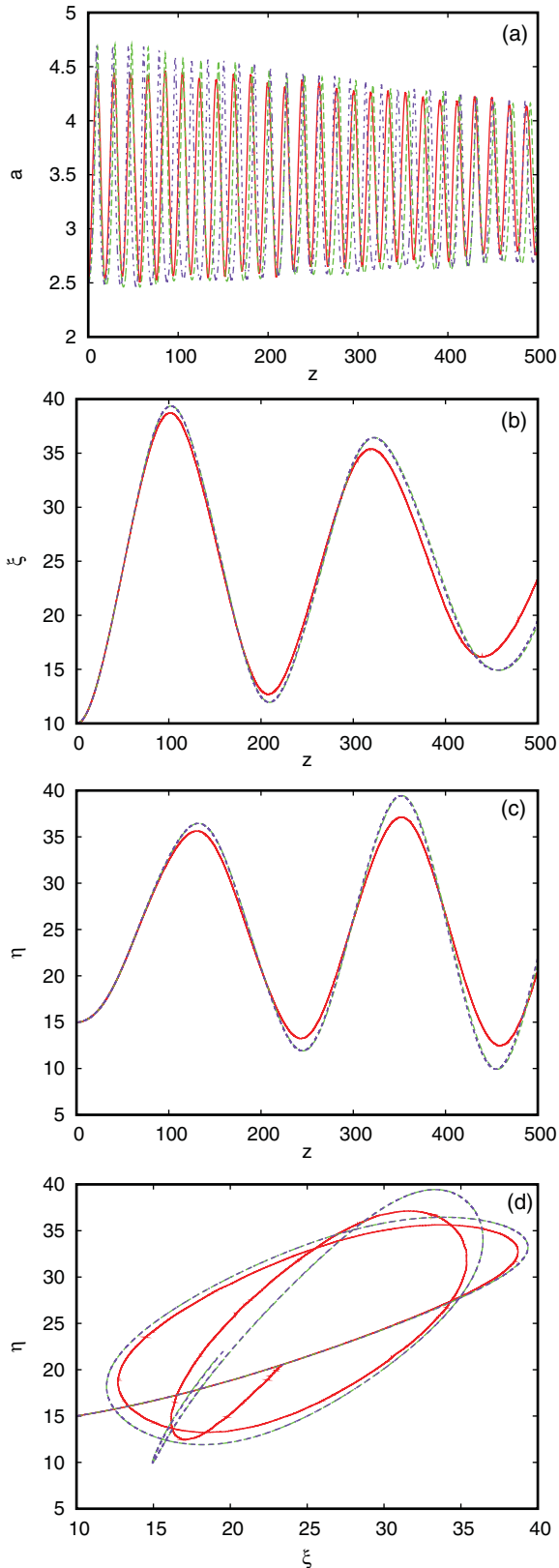
FIG. 2. (Color online) Comparison between the full numerical solution (red solid line), Fourier series solution (green dashed line), and method of images solution (blue dot-dashed line) for the (a) amplitude a, (b) x position, (c) y position, and (d) x-y position for a square cell. The initial values are $a = 2.5$, $w = 4$, $\xi = 10$, $\eta = 15$, $V_x = 0$, and $V_y = 0$ with $\nu = 200$, $L_x = 50$, and $L_y = 50$.

with the numerical solution than the images solution. This is because the modulation equations for the amplitude and width oscillation of the nematicon form a nonlinear oscillator. The period of the amplitude oscillation is then dependent on the amplitude and so the slight amplitude difference between the numerical and modulation solutions translates into a period difference. However, the overall envelope of the amplitude evolution as given by the modulation equations is in excellent agreement with that of the numerical solution, with a slightly higher rate of decay to the steady state. The trajectory of the nematicon as given by both sets of modulation equations is identical, but there is a difference in the amplitude evolution. This is due to all the integrals for the Fourier series solution for the director being evaluated exactly, while the integral with the Green's function, resulting in the solution (18) for θ, had to be evaluated asymptotically. This approximate evaluation had a greater effect on the amplitude than the position. The repulsive effect of the cell walls on the nematicon can be seen from Fig. 2(d) [21,22]. The modulation equations based on the method of images are computationally faster than the Fourier series solution. Since the position is the only data that are experimentally available and the two sets of modulation equations give identical positions, the method of images has an advantage over the Fourier series solution.

Let us now consider the propagation of a nematicon down a more physically realistic rectangular cell. Typical results are shown in Fig. 3. The aspect ratio chosen replicates a case of two-dimensional nematicon propagation studied by Alberucci *et al.* [20]. In this work the propagation was studied numerically and also analytically by assuming that the nematicon motion in the x and y directions could be approximated by two independent one-dimensional motions. The agreement between the modulation and numerical solutions is similar to that for the square cell shown in Fig. 2. The Fourier series and images modulation equations give identical positions, which is in excellent agreement with the position as given by the numerical solution. Again, there is a period difference in the amplitude oscillations as given by the modulation and numerical solutions, which is linked to the small difference in overall amplitude between these oscillations, and the modulation amplitudes decay to the steady state at a slightly faster rate than the numerical amplitude. The major difference in the nematicon propagation between the square and rectangular cells is the fewer y oscillations of the nematicon across the cell due to the increased cell width in the y direction. The agreement in position between the modulation and numerical solutions is much better than for the two independent one-dimensional motion approximation of Alberucci *et al.* [20], as expected because the present theory is fully two dimensional.

A common approximation for the director distribution in a finite cell is to approximate it by the first term in its Fourier series solution [27]. This approximation is of particular importance when nonparaxial effects are studied as it greatly decreases the numerical computation involved as then the Laplacian is in two, not three, dimensions. It is found that numerical solutions of the nonparaxial nematicon equations for the nematicon trajectory under this approximation are in good agreement with experimental results [27]. The validity of this approximation will be studied using the Fourier series
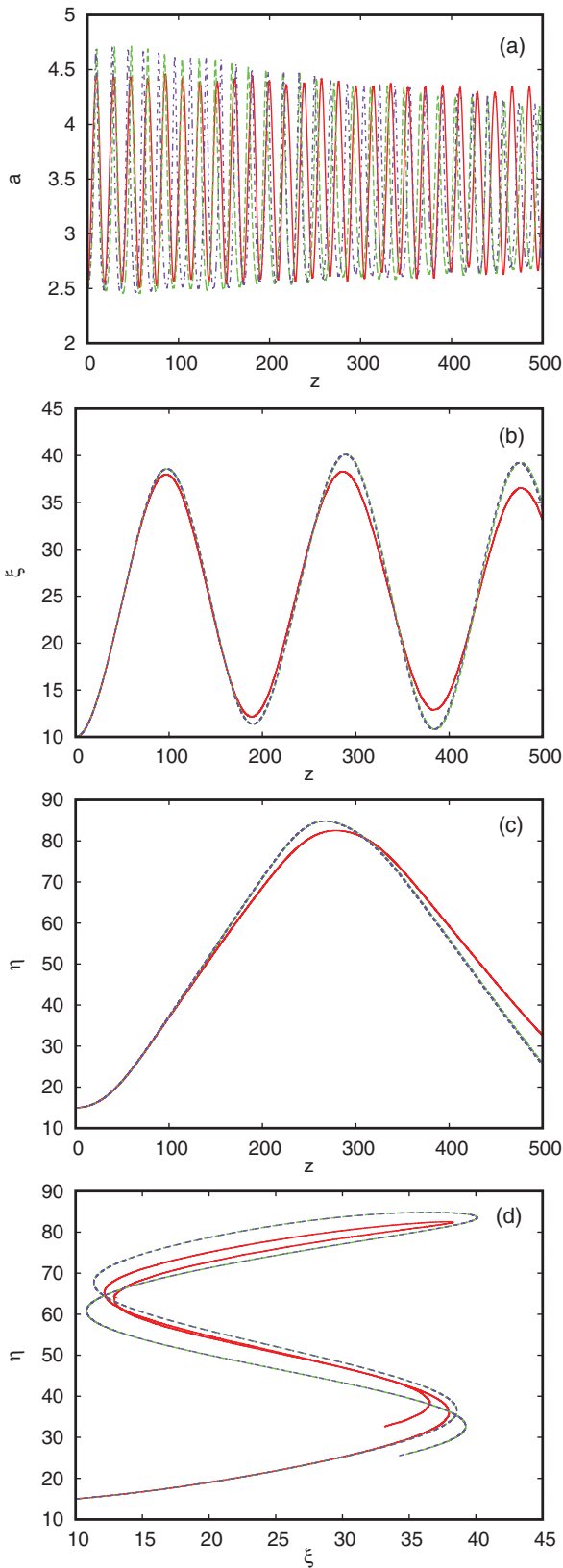
FIG. 3. (Color online) Comparison between the full numerical solution (red solid line), Fourier series solution (green dashed line), and method of images solution (blue dot-dashed line) for the (a) amplitude a, (b) x position, (c) y position, and (d) x-y position for a rectangular cell. The initial values are $a = 2.5$, $w = 4$, $\xi = 10$, $\eta = 15$, $V_x = 0$, and $V_y = 0$ with $\nu = 200$, $L_x = 50$, and $L_y = 100$.

modulation equations of the present work. Figure 4 shows a comparison between the numerical solution of the nematicon equations, the full Fourier series modulation equations solution and the Fourier series modulation equations solution with only the fundamental and the fundamental and first harmonic in the series. It can be seen that the truncated Fourier series results in a poor comparison for the amplitude evolution, but a good comparison for the nematicon trajectory when only the fundamental mode in the Fourier series is used. Paradoxically, when the second harmonic is included the Fourier series gives a much poorer comparison for the nematicon trajectory, while the amplitude comparison improves. This is a consequence of using such low-dimensional approximations to the full series. The comparisons of Fig. 4 show the adequacy of the approximation of Alberucci *et al.* [27] as the numerical and experimental results for the nematicon trajectory are compared, not the beam intensity, which is a more difficult comparison, and only the fundamental mode is used in the approximation.

The approximation of using only a few terms in the series solution for the director can also be applied to the images solution (18) for the director. Figure 5 shows comparisons between the full numerical solution of the nematicon equations and the method of images modulation equations solution with just the first 8 nearest-neighbor images to the physical cell. It can be seen that only these 9 terms (the source plus 8 images) gives an excellent comparison for both the amplitude and position of the nematicon. The reason for this is that the contribution of an image decays both with its distance from the physical cell and the cell dimensions. This shows that, for simplicity, the full images solution does not have to be used and the much simpler approximation of only nearest-neighbor images results in a good approximation.

V. CONCLUSIONS

The propagation of a bulk solitary wave, a nematicon, in a finite nematic-liquid-crystal cell has been investigated. The walls of the cell have been pretreated by rubbing to give the nematic molecules a pretilt in order to overcome the Freédricksz threshold. A hybrid exact solution-modulation theory technique has been used, with the director perturbation resulting from the nematicon being found using two techniques: a Fourier series solution and a Green's function solution based on the method of images. These two solution methods are mathematically equivalent, which can be shown by expressing the Green's function in a Fourier series, or by using the Poisson summation formula, which is equivalent. In application, however, these two techniques have different utility. Both have been found to give solutions in excellent agreement with full numerical solutions of the modulation equations. The major difference comes when only a few terms are used in the series to give simpler approximate solutions. Using only the fundamental or the fundamental plus first harmonic in the Fourier series solution gives an adequate approximation for the trajectory of the nematicon, but not its amplitude (power) evolution. In contrast, using the source plus 8 nearest-neighbor images in the method of images solution gives good approximations to the amplitude and position evolution of the nematicon. The first of these validates an approximation used in the study of nonparaxial effects [27].
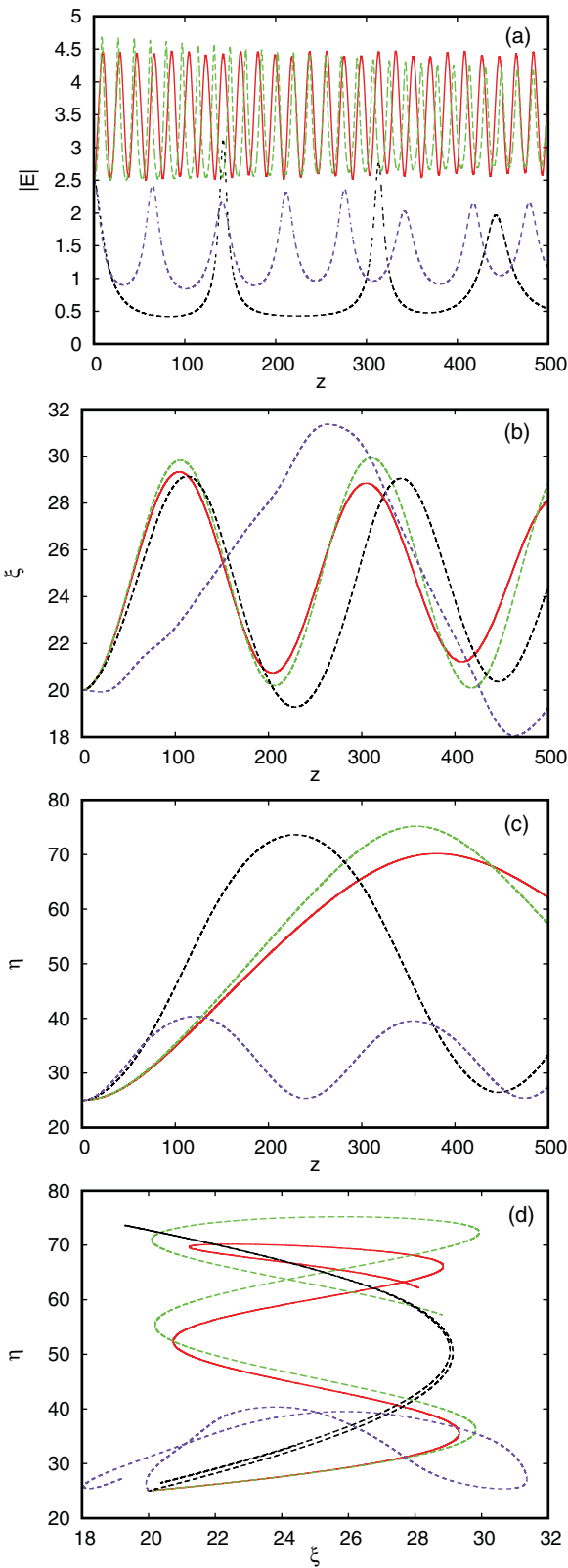
FIG. 4. (Color online) Comparison between the full numerical solution (red solid line), Fourier series solution (green long dashed line), the Fourier series solution with fundamental only (black dashed line), and the fundamental plus second harmonic (blue short dashed line) for the (a) amplitude a, (b) x position, (c) y position, and (d) x-y position for a rectangular cell. The initial values are $a = 2.5$, $w = 4$, $\xi = 20$, $\eta = 25$, $V_x = 0$, and $V_y = 0$ with $\nu = 200$, $L_x = 50$, and $L_y = 100$.
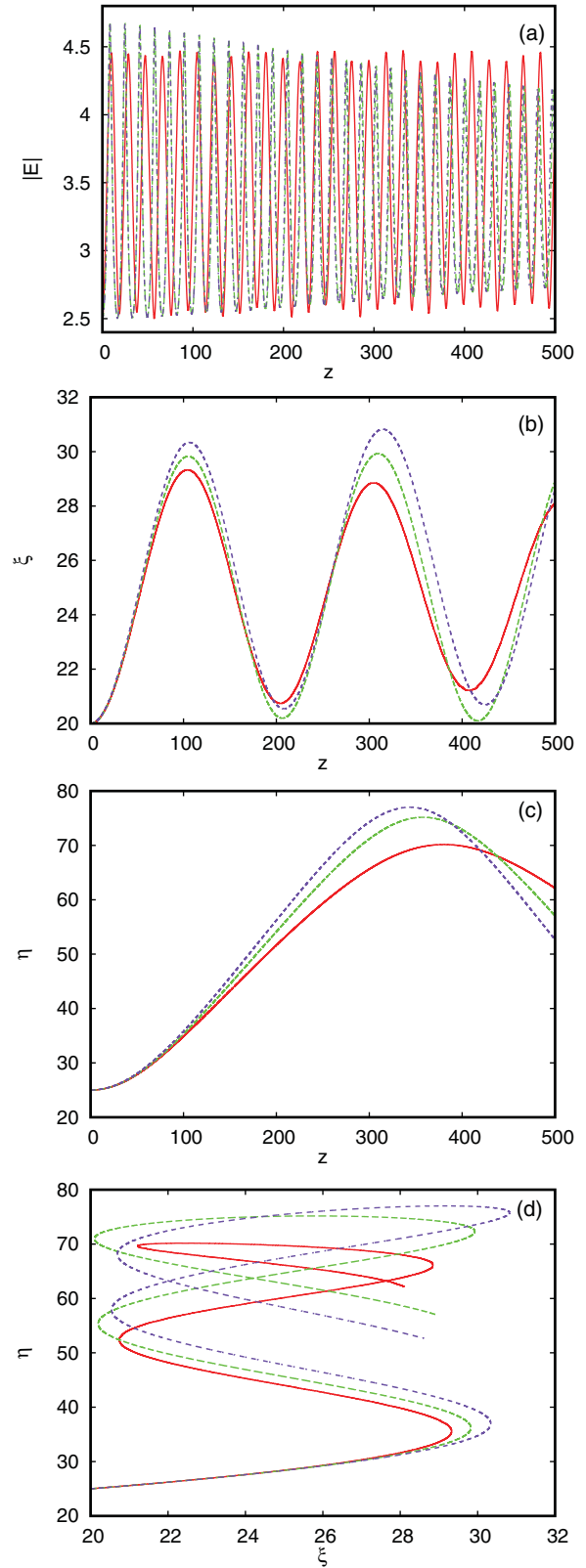
FIG. 5. (Color online) Comparison between the full numerical solution (red solid line), method of images solution (green long dashed line), and method of images solution taking only the first eight images (blue dashed line) for the (a) amplitude a, (b) x position, (c) y position, and (d) x-y position for a rectangular cell. The initial values are $a = 2.5$, $w = 4$, $\xi = 20$, $\eta = 25$, $V_x = 0$, and $V_y = 0$ with $\nu = 200$, $L_x = 50$, and $L_y = 100$.

The present study shows that the method of images, while it has not been widely used to analytically study nematicon evolution, has promise as an alternative to using Fourier series solutions for the director distribution. The bouncing of the nematicon by the cell walls is then clearly seen as the effect of the images. Indeed, this method can be used for the equations describing nonlinear beam evolution in other bulk media [11–18]. In this regard, the view of the effect of the cell walls as due to image sources has promise [47]. The Green's function for the images solution used in the present work was that for the half plane mapped conformally onto a rectangle. This opens the possibility of studying beam evolution in other geometries for which closed form conformal mappings are available. The

further use of the method of images for beam evolution in finite media will be the subject of further work.

APPENDIX A: MODULATION EQUATIONS FOURIER SERIES EXPANSION

Taking variations of the averaged Lagrangian (12) with respect to the nematicon parameters gives the modulation equations for the evolution of the nematicon:

$$\frac{d}{dz}\left[\frac{1}{4}a^2w^2 + \Lambda g^2\right] = 0, \tag{A1}$$

$$\frac{d}{dz}(aw^2) = 2\Lambda g\left[\sigma' - V_x\xi' - V_y\eta' + \frac{1}{2}V_x^2 + \frac{1}{2}V_y^2\right], \tag{A2}$$

$$\frac{d\xi}{dz} = V_x, \quad \frac{d\eta}{dz} = V_y, \tag{A3}$$

$$\frac{d}{dz}\left(\frac{1}{4}a^2w^2 + \Lambda g^2\right)V_x = \frac{2a^4w^4}{\nu L_x^2 L_y}\sum_{n,m=1}^{\infty}\frac{ne^{-2\gamma_1}}{Q_1}\sin\frac{n\pi\xi}{L_x}\cos\frac{n\pi\xi}{L_x}\sin^2\frac{m\pi\eta}{L_y}, \tag{A4}$$

$$\frac{d}{dz}\left(\frac{1}{4}a^2w^2 + \Lambda g^2\right)V_y = \frac{2a^4w^4}{\nu L_x L_y^2}\sum_{n,m=1}^{\infty}\frac{me^{-2\gamma_1}}{Q_1}\sin^2\frac{n\pi\xi}{L_x}\sin\frac{m\pi\eta}{L_y}\cos\frac{m\pi\eta}{L_y}, \tag{A5}$$

$$\frac{dg}{dz} = \frac{a}{2w^2} - \frac{\pi a^3w^4}{2\nu L_x L_y}\sum_{n,m=1}^{\infty}e^{-2\gamma_1}\sin^2\frac{n\pi\xi}{L_x}\sin^2\frac{m\pi\eta}{L_y}, \tag{A6}$$

$$\frac{d\sigma}{dz} = -\frac{2}{w^2} + \frac{1}{2}\left(V_x^2 + V_y^2\right) + \frac{8a^2w^2}{\pi\nu L_x L_y}\sum_{n,m=1}^{\infty}\frac{e^{-2\gamma_1}}{Q_1}\sin^2\frac{n\pi\xi}{L_x}\sin^2\frac{m\pi\eta}{L_y} + \frac{\pi a^2w^4}{\nu L_x L_y}\sum_{n,m=1}^{\infty}e^{-2\gamma_1}\sin^2\frac{n\pi\xi}{L_x}\sin^2\frac{m\pi\eta}{L_y}. \tag{A7}$$

Modulation equation (A1) is the equation for conservation of mass (optical power) and Eqs. (A4) and (A5) are those for conservation of x and y momentum, respectively. The primary concern of the present work is the trajectory of the nematicon, which is given by the modulation equations (A3)–(A5).

As the nematicon evolves it sheds diffractive radiation in order to settle to a steady state [30,42,48]. The flux of diffractive radiation from the nematicon has been calculated previously [30,42,48]. From this previous work we have that, to include loss to diffractive radiation, the mass equation (A1) and the modulation equation (A6) for g become

$$\frac{d}{dz}\left[\frac{1}{4}a^2w^2 + \Lambda g^2\right] = -2\delta\Lambda\kappa^2, \tag{A8}$$

$$\frac{dg}{dz} = \frac{a}{2w^2} - \frac{\pi a^3w^4}{2\nu L_x L_y}\sum_{n=1}^{\infty}\sum_{m=1}^{\infty}e^{-2\gamma_1}\sin^2\frac{n\pi\xi}{L_x}\sin^2\frac{m\pi\eta}{L_y} - 2\delta g. \tag{A9}$$

The loss coefficient δ is

$$\delta = -\frac{\sqrt{2\pi}}{32e\kappa\tilde{\Lambda}}\int_0^z \pi\kappa(z')\ln[(z-z')/\tilde{\Lambda}]\left[\left(\left\{\frac{1}{2}\ln[(z-z')/\tilde{\Lambda}]\right\}^2 + \frac{3\pi^2}{4}\right)^2 + \pi^2\{\ln[(z-z')/\tilde{\Lambda}]\}^2\right]^{-1}\frac{dz'}{(z-z')}, \tag{A10}$$

where

$$\kappa^2 = \frac{1}{\tilde{\Lambda}}\left[\frac{1}{4}a^2w^2 - \frac{1}{4}\hat{a}^2\hat{w}^2 + \tilde{\Lambda}g^2\right]. \tag{A11}$$

One major effect of nonlocality is to shift the point at which the nematicon sheds diffractive radiation from the edge of the shelf $\sqrt{(x-\xi)^2 + (y-\eta)^2} = \ell^2$ to a new radius $\tilde{\ell}$ from the nematicon position (ξ, η), which is the edge of the director response [30]. This radius for the radiation response was termed the outer-shelf radius [30]. In the present case of a finite cell, the director response extends to the cell walls. Hence,

$$\tilde{\ell} = \min\left(\frac{L_x}{2}, \frac{L_y}{2}\right) \tag{A12}$$

and $\tilde{\Lambda} = \tilde{\ell}^2/2$. In the case of a finite cell, the diffractive radiation is then shed in a boundary layer at the cell walls.

APPENDIX B: MODULATION EQUATIONS: METHOD OF IMAGES

Taking variations of the averaged Lagrangian (19) with respect to the nematicon parameters gives the modulation equations for the evolution of the nematicon

$$\frac{d}{dz}\left[\frac{1}{4}a^2 w^2 + \Lambda g^2\right] = 0, \tag{B1}$$

$$\frac{d}{dz}(aw^2) = 2\Lambda g\left[\sigma' - V_x \xi' - V_y \eta' + \frac{1}{2}V_x^2 + \frac{1}{2}V_y^2\right], \tag{B2}$$

$$\frac{d\xi}{dz} = V_x, \quad \frac{d\eta}{dz} = V_y, \tag{B3}$$

$$\frac{d}{dz}\left(\frac{1}{4}a^2 w^2 + \Lambda g^2\right)V_x = \frac{a^4 w^4}{8\nu}\frac{\eta^2}{\xi(\xi^2+\eta^2)} + \frac{a^4 w^4}{8\nu}\sum_{n,m=-\infty}^{\infty}\left[\frac{nL_x - \xi}{(nL_x-\xi)^2 + (mL_y-\eta)^2} - \frac{2\eta nm L_x L_y}{(n^2 L_x^2 + m^2 L_y^2)^2}\right]$$
$$- \frac{a^4 w^4}{8\nu}\sum_{n,m=-\infty}^{\infty}\frac{nL_x - \xi}{(nL_x-\xi)^2 + m^2 L_y^2}, \tag{B4}$$

$$\frac{d}{dz}\left(\frac{1}{4}a^2 w^2 + \Lambda g^2\right)V_y = \frac{a^4 w^4}{8\nu}\frac{\xi^2}{\eta(\xi^2+\eta^2)} + \frac{a^4 w^4}{8\nu}\sum_{n,m=-\infty}^{\infty}\left[\frac{mL_y - \eta}{(nL_x-\xi)^2 + (mL_y-\eta)^2} - \frac{2\xi nm L_x L_y}{(n^2 L_x^2 + m^2 L_y^2)^2}\right]$$
$$- \frac{a^4 w^4}{8\nu}\sum_{n,m=-\infty}^{\infty}\frac{mL_y - \eta}{n^2 L_x^2 + (mL_y-\eta)^2}, \tag{B5}$$

$$\frac{dg}{dz} = \frac{a}{2w^2} - \frac{a^3 w^2}{8\nu}, \tag{B6}$$

$$\frac{d\sigma}{dz} = -\frac{2}{w^2} + \frac{1}{2}(V_x^2 + V_y^2) + \frac{a^2 w^2}{\nu}\left[-\Delta_1 - \Delta_2 + \Delta_3 + \Delta_4 + \frac{1}{4}\right]. \tag{B7}$$

Modulation equation (B1) is the equation for conservation of mass (optical power) and Eqs. (A4) and (B5) are those for conservation of x and y momentum, respectively. The primary concern of the present work is the trajectory of the nematicon, which is given by the modulation equations (B3)–(B5).

As the nematicon evolves it sheds diffractive radiation in order to settle to a steady state [30,42,48]. As in Appendix A, the modulation equations (B1) and (B6) are modified to become

$$\frac{d}{dz}\left[\frac{1}{4}a^2 w^2 + \Lambda g^2\right] = -2\delta\Lambda\kappa^2, \tag{B8}$$

$$\frac{dg}{dz} = \frac{a}{2w^2} - \frac{a^3 w^2}{8\nu} - 2\delta g. \tag{B9}$$

The loss coefficient δ is given by (A10), with $\tilde{\Lambda}$ given by (A12).

[1] C. Conti, M. Peccianti, and G. Assanto, Phys. Rev. Lett. **91**, 073901 (2003).

[2] G. Assanto, M. Peccianti, and C. Conti, Opt. Photonics News **14**, 44 (2003).

[3] Yu. S. Kivshar and G. Agrawal, *Optical Solitons: From Fibers to Photonic Crystals* (Academic Press, San Diego, 2003).

[4] M. Peccianti, A. de Rossi, G. Assanto, A. de Luca, C. Umeton, and I. C. Khoo, Appl. Phys. Lett. **77**, 7 (2000).

[5] C. Conti, M. Peccianti, and G. Assanto, Phys. Rev. Lett. **92**, 113902 (2004).

[6] M. Peccianti, A. Pasquazi, G. Assanto, and R. Morandotti, Opt. Lett. **35**, 3342 (2010).

[7] G. Assanto, A. Fratalocchi, and M. Peccianti, Opt. Express **15**, 5248 (2007).

[8] O. Bang, W. Krolikowski, J. Wyller, and J. J. Rasmussen, Phys. Rev. E **66**, 046619 (2002).

[9] C. Rotschild, O. Cohen, O. Manela, M. Segev, and T. Carmon, Phys. Rev. Lett. **95**, 213904 (2005).

[10] P. D. Rasmussen, O. Bang, and W. Z. Królikowski, Phys. Rev. E **72**, 066611 (2005).

[11] N. I. Nikolov, D. Neshev, O. Bang, and W. Z. Królikowski, Phys. Rev. E **68**, 036614 (2003).

[12] B. Alfassi, C. Rotschild, O. Manela, M. Segev, and D. N. Christodoulides, Opt. Lett. **32**, 154 (2007).

[13] I. C. Khoo, Phys. Rep. **471**, 221 (2009).

[14] E. A. Kuznetsov and A. M. Rubenchik, Phys. Rep. **142**, 103 (1986).

[15] C. Rotschild, M. Segev, Z. Xu, Y. V. Kartashov, L. Torner, and O. Cohen, Opt. Lett. **31**, 3312 (2006).

[16] C. Rotschild, B. Alfassi, O. Cohen, and M. Segev, Nature Phys. **2**, 769 (2006).

[17] W. Wan, S. Jia, and J. W. Fleischer, Nature Phys. **3**, 46 (2007).

[18] W. Wan, D. V. Dylov, C. Barsi, and J. W. Fleischer, *OSA/CLEO/IQEC 2009*.

[19] I. C. Khoo, *Liquid Crystals: Physical Properties and Nonlinear Optical Phenomena* (Wiley, New York, 1995).

[20] A. Alberucci, G. Assanto, D. Buccoliero, A. S. Desyatnikov, T. R. Marchant, and N. F. Smyth, Phys. Rev. A **79**, 043816 (2009).

[21] A. Alberucci and A. Assanto, J. Opt. Soc. Am. B **24**, 2314 (2007).

[22] A. Alberucci, M. Peccianti, and G. Assanto, Opt. Lett. **32**, 2795 (2007).

[23] D. Buccoliero, A. S. Desyatnikov, W. Krolikowski, and Y. S. Kivshar, J. Opt. A: Pure Appl. Opt. **11**, 094014 (2009).

[24] Y. V. Izdebskaya, V. G. Shvedov, A. S. Desyatnikov, W. Krolikowski, and Y. S. Kivshar, Opt. Lett. **35**, 1692 (2010).

[25] Y. V. Izdebskaya, V. G. Shvedov, A. S. Desyatnikov, W. Z. Krolikowski, M. Belic, G. Assanto, and Y. S. Kivshar, Opt. Express **18**, 3258 (2010).

[26] Y. V. Izdebskaya, V. Shvedov, A. Desyatnikov, W. Krolikowski, G. Assanto, and Y. Kivshar, J. Eur. Opt. Soc. Rapid Pub. **5**, 10008 (2010).

[27] A. Alberucci, A. Piccardi, M. Peccianti, M. Kaczmarek, and G. Assanto, Phys. Rev. A **82**, 023806 (2010).

[28] A. Alberucci and G. Assanto, Opt. Lett. **36**, 334 (2011).

[29] R. Courant and D. Hilbert, *Methods of Mathematical Physics* (Interscience Publishers, New York, 1965), Vol 1.

[30] A. A. Minzoni, N. F. Smyth, and A. L. Worthy, J. Opt. Soc. Am. B **24**, 1549 (2007).

[31] G. Assanto, A. A. Minzoni, M. Peccianti, and N. F. Smyth, Phys. Rev. A **79**, 033837 (2009).

[32] M. Peccianti, A. Fratalocchi, and G. Assanto, Opt. Express **12**, 6524 (2004).

[33] B. D. Skuse and N. F. Smyth, Phys. Rev. A **79**, 063806 (2009).

[34] G. B. Whitham, *Linear and Nonlinear Waves* (J. Wiley and Sons, New York, 1974).

[35] C. García Reimbert, A. A. Minzoni, T. R. Marchant, N. F. Smyth, and A. L. Worthy, Physica D **237**, 1088 (2008).

[36] B. D. Skuse and N. F. Smyth, Phys. Rev. A **77**, 013817 (2008).

[37] G. Assanto, B. D. Skuse, and N. F. Smyth, Photon. Lett. Poland **1**, 154 (2009).

[38] G. Assanto, B. D. Skuse, and N. F. Smyth, Phys. Rev. A **81**, 063811 (2010).

[39] G. Assanto, A. A. Minzoni, N. F. Smyth, and A. L. Worthy, Phys. Rev. A **82**, 053843 (2010).

[40] A. A. Minzoni, N. F. Smyth, and Z. Xu, Phys. Rev. A **81**, 033816 (2010).

[41] A. W. Snyder and M. J. Mitchell, Science **276**, 1538 (1997).

[42] W. L. Kath and N. F. Smyth, Phys. Rev. E **51**, 1484 (1995).

[43] J. Yang, Stud. Appl. Math. **98**, 61 (1997).

[44] D. E. Pelinovsky and Y. Yang, Stud. Appl. Math. **105**, 245 (2000).

[45] M. J. Ablowitz, S. D. Dixon, T. P. Horikis, and D. J. Frantzeskakis, Proc. R. Soc. London A **467**, 2597 (2011).

[46] A. A. Minzoni, N. F. Smyth, A. L. Worthy, and Y. S. Kivshar, Phys. Rev. A **76**, 063803 (2007).

[47] A. A. Minzoni, L. W. Sciberras, N. F. Smyth, and A. L. Worthy, Nematicons: Spatial Optical Solitons in Nematic Liquid Crystals, edited by G. Assanto (John Wiley and Sons, Hoboken, New Jersey, in press).

[48] C. García Reimbert, A. A. Minzoni, and N. F. Smyth, J. Opt. Soc. Am. B **23**, 294 (2006).